JOURNAL OF CATALYSIS 108, 214–232 (1987)

Metals Contamination of Aluminosilicate Cracking Catalysts by Ni- and VO-Tetraphenylporphin

S. A. ROTH,*,†,[1] L. E. ITON,* T. H. FLEISCH,‡ B. L. MEYERS,‡ C. L. MARSHALL,‡ AND W. N. DELGASS†

*Argonne National Laboratory, Argonne, Illinois 60439; ‡Amoco Research Center, Naperville, Illinois 60566; and †School of Chemical Engineering, Purdue University, West Lafayette, Indiana 47907

Received April 6, 1987; revised June 22, 1987

The interaction of nickel and vanadyl tetraphenylporphin with amorphous silica–alumina, Y zeolite, and a cracking catalyst containing 15% Y zeolite has been studied with a variety of techniques. For the porphins on the silica–alumina and the cracking catalyst, electronic photoacoustic absorption spectrometry (EPAS), electron paramagnetic resonance (EPR) on V, X-ray photoelectron spectroscopy (XPS), and plasma desorption mass spectrometry (PDMS) confirm interaction of molecularly dispersed porphin molecules with the support but show no demetallation at temperatures below 120°C. The latter result is supported by EPAS findings of nearly quantitative desorption of the intact metal prophin after redissolution of the impregnated supports. Since the large porphin molecules cannot fit into the intracrystalline pore structure of the zeolite, the effective loading of those samples was several monolayers. Spectroscopic measurements showed, and scanning electron microscopy confirmed that the porphins form crystallites in this case. Blockage of a substantial portion of the external surface of the zeolite particles was indicated, however, by a large reduction in the measured intracrystalline pore volume after porphin impregnation. Infrared spectroscopy showed that porphin decomposition during calcination in air begins at 200–300°C. On the amorphous silica–alumina-containing materials, the decomposition extends over a 150°C range during programmed heating. Metal porphins on the zeolite support showed a sharp, apparently catalytic, exotherm and weight loss at a temperature more than 100°C higher than that for the onset of loss of molecular structure. These results show that interactions of metal porphins with cracking catalysts and their individual components are a strong function of coverage and that the decomposition of the porphins can be influenced by that interaction.

INTRODUCTION

Naturally abundant nickel and vanadium complexes, present in heavy crude oil feeds in the form of metalloporphins, decompose on the surface of petroleum cracking catalysts leading to both catalyst deactivation and loss of selectivity (*1–3*). The major deleterious effects of the metals are a loss in conversion to gasoline products accompanied by a simultaneous increase in hydrogen and coke production. As the current interest in refining metal-containing residual feedstocks has grown, there has been a renewal of research activity toward the characterization of metal-poisoned fluid catalytic cracking (FCC) catalysts and an increased interest in the development of metals-resistant FCC catalysts.

Modern, commercial cracking catalysts are composed of 10–15% rare-earth or ultrastable Y zeolite embedded in an amorphous silica–alumina matrix. In attempts to model the poisoning effects of metals on amorphous cracking catalysts (*4–6*) and modern, zeolitic FCC catalysts (*7*), various methods for artificial metals contamination have been developed. Usually catalysts have been impregnated with aqueous solutions of metal salts (*6, 8, 9*) or organic solutions of metal naphthenates

[1] Present address: Johnson Mathey, Inc., Wayne, PA 19087-1816.

0021-9517/87 $3.00

(*10–17*). The general conclusions concerning the effect of metal poisoning on zeolitic cracking catalysts may be separated into the individual effects of nickel and vanadium contamination (*2*). Nickel does not greatly affect conversion levels, but, being a dehydrogenation catalyst under these conditions, it is effective for both coke and hydrogen production as well as the increase in the olefin content of the product. Vanadium is especially deleterious because it appears to attack the zeolite component of the catalyst, destroying its crystallinity and resulting in a dramatic decrease in cracking activity (*18, 19*).

In this work, a multivariant approach in which a variety of analytical tools could be employed to provide insight into the problem of metals contamination of cracking catalysts was designed. To understand the role of nickel and vanadium contaminants in the deactivation of composite cracking catalysts, it was first deemed necessary to understand the interaction of the individual contaminants on each component of the catalyst. Therefore, rare-earth Y zeolite and amorphous silica–alumina were impregnated separately with toluene solutions of a model organometallic contaminant. Since the metallic species in crude oil have been identified as being metalloporphyrins (*20, 21*), realistic model poisons, i.e., nickel and vanadyl *meso*-tetraphenylporphins, have been employed. This initial investigation has involved the surface characterization of adsorbed metalloporphins at realistic metal contamination levels. Since reactor equilibrium FCC catalysts are only allowed to accumulate metals to approximately 5000 ppm Ni and/or 8000 ppm V, the maximum metalloporphin loadings have been kept at or below this contamination level.

EXPERIMENTAL METHODS

Materials

Two aluminosilicates were utilized as starting materials for the preparation of catalysts inpregnated with metalloporphin model poisons. Na–Y zeolite was obtained from Union Carbide Corp. (as LZ-Y-52, Lot No. 7458-11A). It was dried at 120°C before direct impregnation. Amorphous silica–alumina was obtained from Amoco Oil Corp. as a 4.67 wt% solids, aqueous gel. It was prepared using the hydrogel procedure described by Magee and Blazek (*22*), in which sodium silicate and aluminum sulfate were coprecipitated producing a 4.97 : 1 ratio of silica to alumina (i.e., Si/Al = 2.48). Before porphin impregnation, the amorphous silica–alumina was filtered, dried at 120°C, and ground into powder form using a mortar and pestle.

Metal-free *meso*-tetraphenylporphin (H_2-TPP) was purchased from Strem Chemicals, Inc., and was used as received. Preparation of nickel *meso*-tetraphenylporphin (Ni-TPP) and vanadyl *meso*-tetraphenylporphin (VO-TPP) was by the method of Adler (*23, 24*). A stoichiometric quantity of nickel acetylacetonate or a tenfold excess of vanadyl sulfate was added to a solution of H_2-TPP in refluxing dimethylforamide (DMF, 2.0 g in 750 ml). The metalloporphin was precipitated from solution by addition of water and was purified by alumina dry column chromatography.

Preparation of Nd–Y Zeolite

Nd–Y zeolite was prepared from Na–Y by exhaustive ion exchange using aqueous solutions of $Nd(NO_3)_3 \cdot 6H_2O$ purchased from AESAR (99.99% reaction grade, batch No. R2454). To an aqueous $Nd(NO_3)_3$ solution (750 ml, 5.8×10^{-2} *M* in distilled, deionized water) was added Na–Y zeolite (20.0 g) and the resulting suspension was magnetically stirred under reflux conditions for 2 h. After the suspension cooled and settled, the supernate was removed by siphonation. The ion exchange was repeated two times with fresh $Nd(NO_3)_3$ solution and then the product was washed three times under reflux with pure water. The partially exchanged Na, Nd–Y zeolite was filtered onto a fine, sintered glass frit, dried at 120°C for 3 h and then calcined under

shallow bed conditions in a 50 ml/min flow of dry air at 750°C for 4 h. After calcination, to allow complete exchange of residual sodium cations (*22*), the zeolite was ion exchanged three additional times and finally washed three times with pure water to remove excess $Nd(NO_3)_3$. Analysis for residual Na by atomic adsorption showed 0.4 wt% Na_2O, corresponding to <2 Na^+ cations per unit cell.

Preparation of 15% Nd–Y:85% Amorphous Silica–Alumina FCC Catalyst

A standard procedure for preparation of zeolitic FCC catalysts was followed (*22*). To an aqueous gel of amorphous silica–alumina (230 g of 4.67% solids) in a 500-ml nalgene beaker was slowly added Nd–Y zeolite (2.00 g, predried at 120°C). After mechanical stirring at 1500 rpm for 30 min with a Teflon-coated rotor, the slurry was filtered through a 150-ml fine sintered glass frit using a water aspirator. The resulting gel was dried at 120°C for 48 h producing a dried cake which was then ground to a fine powder before impregnation with porphins. Quantitative X-ray powder diffraction analysis of the 22.8° 2θ line, using Nd–Y as a 100% standard and accounting for differences in the X-ray mass absorption coefficients (*25*), yielded 14.9% Nd–Y zeolite as compared to the theoretical value of 15.6% Nd–Y based on the weight fractions added to the slurry.

Addition of Porphins to the Catalysts

Method I: Incipient wetness impregnation. To a 50-ml Kjeldahl flask, equipped with a side arm and a Teflon vacuum stopcock, was added 2.00 g of an aluminosilicate (predried at 120°C) and a Teflon-coated stirring bar. Through an O-ring universal adaptor was attached a 15-ml burette having a Teflon vacuum stopcock between the burette tip and the top of the flask. A concentrated porphin/toluene solution ($\sim 3 \times 10^{-4}$ *M*) was added dropwise onto the aluminosilicate with continuous stirring until incipient wetness (~1 ml). Then the stopcock above the flask was closed and the solvent was removed under vacuum through the side arm. A liquid nitrogen trap was placed between the Kjeldahl flask and the vacuum line for solvent condensation. This procedure was repeated until the desired metalloporphin loading was obtained (~120 ml for 1% porphin loading). The impregnated sample was dried at 120°C for 15 h in air before further analysis.

Method II: Slurry impregnation. To a 250-ml Kjeldahl flask, equipped with a side arm and a Teflon vacuum stopcock, was added 2.00 g of an aluminosilicate (predried at 120°C), a Teflon-coated stirring bar, ~200 ml of concentrated porphin/toluene solution ($\sim 3 \times 10^{-4}$ *M*), and finally a Teflon stopper. With continuous stirring, the solvent was vacuum transferred through the side arm into an adjacent liquid nitrogen trap. This procedure was repeated until the desired metalloporphin loading was obtained (~600 ml for 5% porphin loading). The resulting powder was dried under vacuum for 1 h and in air at 120°C for 15 h to remove excess toluene.

Instrumentation

The electronic absorption spectra of porphins in solution between 200 and 900 nm were obtained using a Beckman Model 25 UV–Vis spectrophotometer. For solid samples, the electronic absorption spectra of impregnated porphins between 200 and 2600 nm were measured using a Princeton Applied Research Model 6001 EG & G photoacoustic spectrometer. Spectra of powdered samples were recorded in air against a carbon black reference at 40 Hz modulation of the incident radiation using the in-phase component of the acoustic signal.

X-band electron paramagnetic resonance spectra of adsorbed VO-TPP were recorded at ~9.15 GHz, between 77 and 300 K using a Varian E-112 spectrometer. Samples degassed by the freeze–pump–thaw method were sealed in quartz tubes for the mea-

surements, and a strong pitch sample was used as a g-value reference ($g = 2.0028$).

X-ray photoelectron spectra were measured with a Hewlett–Packard Model 5950B spectrometer using monochromatic AlK_α radiation ($h\nu = 1486.6$ eV). Low-energy electrons supplied by an electron flood gun minimized sample charging. Samples were pressed into self-supporting wafers at 10,000 psig before analysis. The recorded photoelectron binding energies (B.E.) were referenced against the Si 2p line at 102.8 eV. The validity of this reference for these catalyst systems was confirmed by the achievement of a constant Al 2p photoelectron binding energy of 74.5 ± 0.2 eV on all sample surfaces.

The specific surface area in square meters per gram and the pore size distribution from 10 to 600 Å radius were calculated from nitrogen adsorption/desorption isotherms obtained at liquid nitrogen temperature on an automated Digisorb 2500 (Micromeritics Instrument Corp.). For measurements on pure supports, ~150 mg of sample were pretreated at 250°C and less than 10^{-4} Torr for 6 h. Porphin-impregnated samples were pretreated at only 110°C to avoid decomposition. The BET equation was employed to calculate specific areas (*26*). Pore size distributions were calculated using the method of Roberts (*27*) and micropore volumes were extrapolated from the slopes of conventional t-plots (*28*).

Scanning electron micrographs of supported metalloporphins were obtained on a JEOL JSM-35C scanning electron microscope. Samples were prepared by pipetting a diethyl ether slurry onto a polished graphite sample holder. Micrographs were obtained at 15 keV. Elemental composition was measured by energy-dispersive X-ray analysis using the ZAF subroutine.

Plasma desorption mass spectra (PDMS) of VO-TPP and Ni-TPP adsorbed on amorphous silica–alumina were analyzed using a californium-252 fission source and a time-of-flight mass spectrometer (*29*). The powdered sample was transferred to the sample plate in the form of an aqueous slurry. Since the porphins are insoluble in water they must remain attached to the solid support during transfer. In the instrument, the sample was bombarded with primary fast fission fragments and the desorbed molecular ions were accelerated through a potential grid and mass analyzed by their times of flight.

The decomposition of adsorbed metalloporphins in air was monitored using a Perkin–Elmer 1700 differential thermal analysis (DTA) system. Temperature programming rates of 0.2–20°C/min were maintained using the system 7/4 control module. Sample weights of 2–3 mg and air flow rates of 30 ml/min were used to eliminate diffusion problems. Thermal gravimetric analysis (TGA) was performed on a Dupont 1090 system using approximately 10 mg of sample and a dry air flow rate of 30 ml/min.

Fourier transform infrared (FTIR) spectra were recorded using a Digilab FTS14 spectrometer. Samples were pressed into KBr pellets at 10,000 psig. Before pellet pressing, limited mixing of sample and dry KBr was performed using a mortar and pestle. Extensive ball milling was found to result in loss of the porphin spectra.

RESULTS AND DISCUSSION

Realistic model poisons, actual nickel(II) and vanadyl(IV) porphins, are being utilized for the first time in a fundamental study of the poisoning of cracking catalysts (Wei *et al.* (30–32) have recently studied the demetallization of metalloporphins on HDS catalysts under reducing conditions). In order to completely characterize metals contamination of zeolite-containing cracking catalysts, it is necessary to determine the distribution of metals on the catalysts. The contaminants may be initially deposited uniformly on both the zeolite and the amorphous silica–alumina matrix or nonuniformly, with a preference for only one component. This initial distribution

may effect the decomposition pathway and ultimately control the extent of poisoning by determining the oxidation state, cluster size, and placement of the metal poison. Toward the goal of understanding this distribution, we initially impregnated the porphins on the individual components of the catalyst and analyzed them.

The surface areas of the two catalyst components were measured by nitrogen adsorption. Although the N_2 uptake or one-point BET surface areas are similar (454 m^2/g for the amorphous silica–alumina and 521 m^2/g for Nd–Y zeolite) it must be recognized that application of the BET equation to zeolites is inappropriate due to capillary condensation in the micropores. A more meaningful measurement of the mesoporous area accessible through pores of radius >10 Å is shown in Fig. 1. For the amorphous silica–alumina, essentially all the surface area is accessible; while for Y zeolite most of the surface is internal, within the extensive microporous structure. In Y zeolite, the entrance to the internal cages is via a "window" of only 7.4 Å in diameter, and therefore, only ~27 m^2/g of external surface area is actually accessible to the 15.4-Å-diameter tetraphenylporphin.

The RE–Y utilized as a component in many industrial FCC catalysts contains a mixture of rare-earth (RE) cations, principally La^{3+} and Ce^{3+}. These trivalent cations stabilize the zeolite structure toward thermal and hydrothermal degradation (*22*). However, they often complicate spectroscopic analyses of metal poisons by obscuring the pertinent metal X-ray absorption or X-ray photoelectron lines (*33, 34*). Since substitution of other trivalent RE^{3+} cations can accomplish the same structural purpose, in this study the Y zeolite was completely exchanged with Nd^{3+}. The impregnation of Ni-TPP and VO-TPP on a Nd–Y zeolite allows for the first time unimpeded X-ray photoelectron spectra (XPS) to be obtained on nickel contaminants, and X-ray absorption spectra to be obtained on vanadium contaminants.

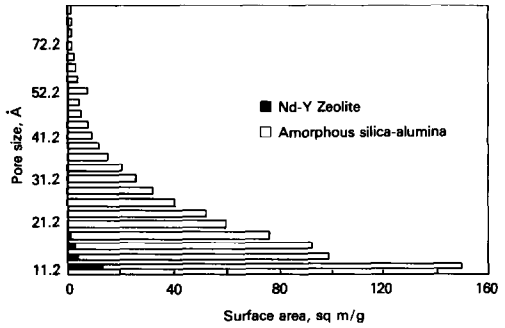

FIG. 1. Comparative surface area (m^2/g) as a function of average pore radius (Å) for (□) amorphous silica–alumina and (■) Nd–Y zeolite.

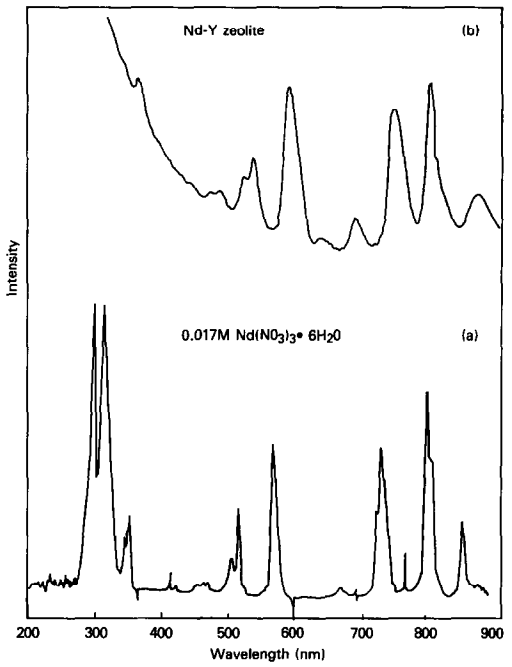

FIG. 2. Comparison between (a) the electronic absorption spectrum of 0.017 *M* aqueous $Nd(NO_3)_3 \cdot 6H_2O$, and (b) the electronic photoacoustic spectrum of Nd–Y zeolite.

The solution electronic spectrum of aqueous Nd^{3+}, an ion with $^4I_{9/2}$ ground state (*35, 36*), is given in Fig. 2*a*. The electronic photoacoustic spectrum (EPAS) of Nd–Y zeolite, Fig. 2*b*, shows that the rare-earth

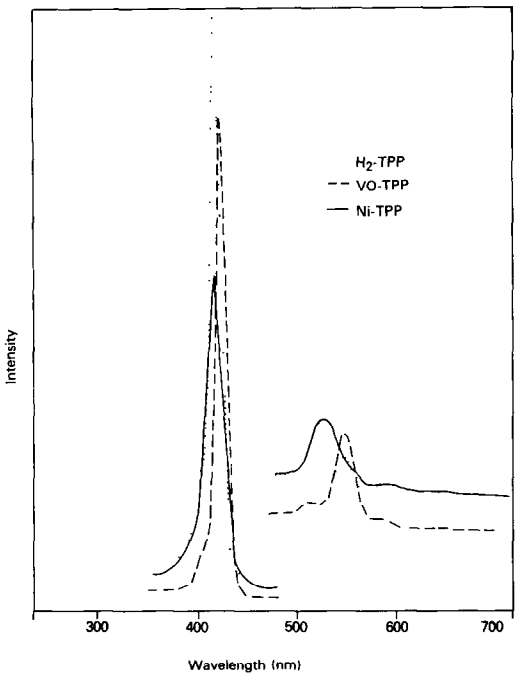

FIG. 3. Solution electronic absorption spectra of 4×10^{-6} *M* porphins in toluene: (—) H_2-TPP, (– – –) VO-TPP, and (···) Ni-TPP.

cation has a crystal field configuration in solution similar to that in the hydrated form of the zeolite.

Electronic absorption spectra of adsorbed porphins. The porphins used as model contaminants have electronic $\pi \rightarrow \pi^*$ transitions in the UV–Vis region (*37–39*), which produce a very intense Soret (*B*) band at ~400 nm and partially allowed transitions (*Q*) in the visible region between 500 and 650 nm which are characteristic of the specific porphin (see Fig. 3). As shown in Fig. 4, the same absorption bands are observed in the electronic photoacoustic spectra (EPAS) of dilute porphins (~0.2 wt%) adsorbed on the surface of Na–Y zeolite. Na–Y was utilized for this experiment so that the porphin transitions would not be obscured by those of the Nd^{3+} cation. The conclusion may be drawn that the porphins under these conditions are molecularly dispersed, although differences in relative intensity between Soret and visible bands suggest some mechanism of intensity borrowing, possibly due to perturbations in the conjugated ring structure. This appears to be typical for TPP complexes upon adsorption. Similar intensity changes have been observed previously for Ni-TPP adsorbed on γ-Al_2O_3 (*40*) and for Co-TPP adsorbed on TiO_2 (*41*) and SiO_2 (*42*) as measured by diffuse reflectance spectroscopy, but no explanations were advanced in those studies.

Deviations from the characteristic, molecular electronic spectra are observed at higher loadings. In the case of Ni-TPP/Na-Y, at loadings less than one monolayer on the external surface (~0.6 wt% Ni-TPP) the spectrum appears to be similar to that of the molecularly dispersed Ni-TPP. However, at high loadings, as seen in Fig. 5, the structure in the longer wavelength portion of the absorption spectrum appears more reminiscent of that of the metal-free porphin. The two porphin deposition tech-

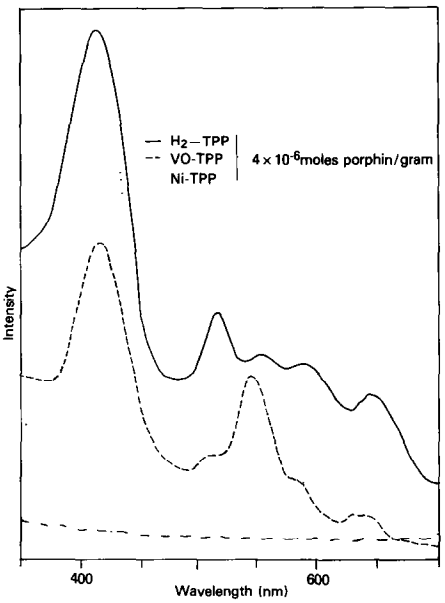

FIG. 4. Electronic photoacoustic spectra of low-loading porphins (~0.2 wt%) supported on Na–Y zeolite: (—) H_2-TPP, (– – –) VO-TPP, (···) Ni-TPP, and (–·–·–) background spectra of Na-Y zeolite.

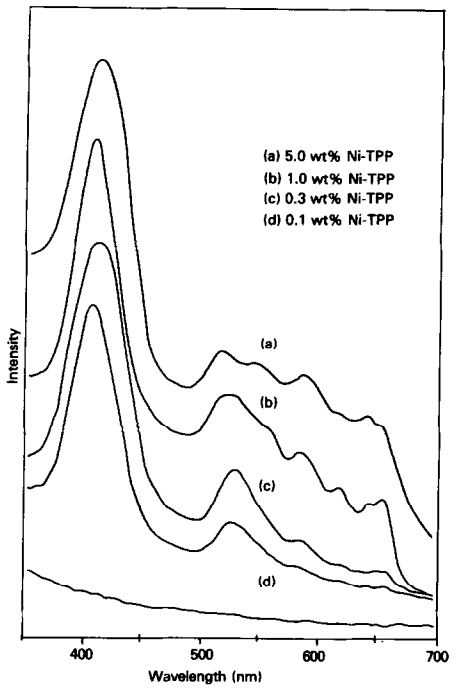

FIG. 5. Electronic photoacoustic spectra of Ni-TPP supported on Na–Y zeolite: (a) 5.0 wt%, (b) 1.0 wt%, (c) 0.3 wt%, and (d) 0.1 wt%. The background spectrum of Na–Y zeolite is also shown.

niques result in impregnated samples with identical EPA spectra. Due to the ease of the slurry impregnation method, it was employed for all loadings greater than 1 wt% porphin. It will be shown that the spectrum at a high loading can be explained as a summation of the spectrum of the dilute, molecularly isolated species plus a new absorption due to a modification of the electronic structure caused by formation of an aggregated porphin system. The spectra of VO-TPP and Ni-TPP adsorbed on amorphous silica–alumina also change as a function of loading, as shown in Fig. 6. Mitchell *et al.* (*43*) observed a similar change in the diffuse reflectance spectrum of VO-TPP adsorbed on fluorided silica and attributed this change to demetallation followed by acidification to form adsorbed H_4-TPP^{2+}. We do not consider this to be the case in our experiments (vide infra).

It was not possible to obtain EPA spectra of the optically opaque, pure porphins. As described by Rosencwaig and Gersho (*44*), if the thermal diffusion length is greater than the optical absorption length, then the acoustic signal will be independent of the absorption coefficient. If the porphin is physically mixed with the support, the thermal diffusion length is apparently shortened and the EPA spectra for the solid porphins at the appropriate concentrations are shown in Fig. 7. The EPA spectra of porphin-impregnated supports, at the same high loadings, also show the increase in absorption in the 500 to 650-nm region and similarity to Fig. 7. Since any aggregated porphin system with porphin–porphin intermolecular interactions will likely produce this change in electronic structure, the porphins may be deposited in either multilayers or crystallites on the high-loading samples.

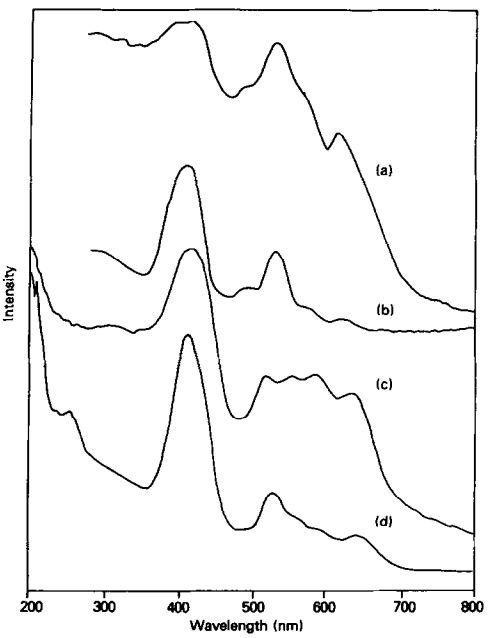

FIG. 6. Electronic photoacoustic spectra of M-TPP supported on amorphous silica–alumina: (a) 8.0 wt% VO-TPP, (b) 0.2 wt% VO-TPP, (c) 5.0 wt% Ni-TPP, and (d) 0.2 wt% Ni-TPP.

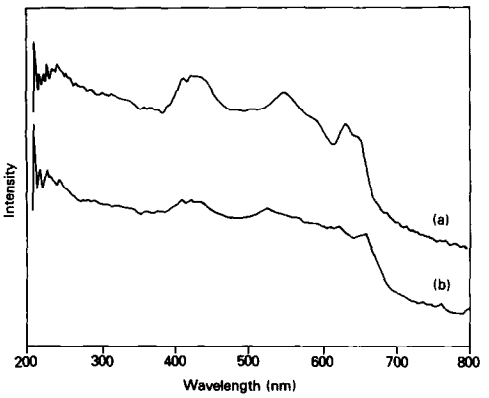

FIG. 7. Electronic photoacoustic spectra of physical mixtures of M-TPP with amorphous silica–alumina: (a) 10.0 wt% VO-TPP, and (b) 5.0 wt% Ni-TPP.

To determine whether the impregnation of porphins results in encapsulation of the zeolite, the micropore volume for a Nd–Y zeolite was measured both before and after deposition of 5 wt% Ni-TPP (see Table 1). The micropore volume is indicative of the volume inside the zeolitic crystallites accessible to nitrogen after extended equilibration. The decrease from 0.232 to 0.094 cc/g must be due to pore mouth blockage. Since the blockage can inhibit removal of toluene during pretreatment as well as prevent penetration of N_2, quantitative evaluation of the degree of encapsulation cannot be made. It is clear, however, that the 60% loss of the three-dimensional, interconnected pore volume of the zeolite implies substantial coverage of the entire surface of a majority of the zeolite particles. After a 4-h calcination at 500°C, the porphin was decomposed and the micropore volume was restored (see Table 1).

Desorption of impregnated porphins. Direct evidence for the porphin staying intact on the surface without demetallation arises from two types of desorption experiments. First, when the supported metalloporphin on either the zeolite or the amorphous silica–alumina was reslurried in toluene, the porphin redissolved into solution. The solution spectrum of the desorbed porphin shows that greater than 90% of the metalloporphin was recovered and provides no evidence for the presence of metal-free porphin. It seems unlikely that a demetallation process would be completely reversible or that it would only occur when more than a monolayer was adsorbed.

Both VO-TPP and Ni-TPP adsorbed on amorphous silica–alumina were analyzed by ^{252}Cf plasma desorption mass spectrometry (PDMS) (*45*). As seen in Fig. 8 the presence of the molecular ion (the highest mass peak in each spectrum) and its fragmentation products implies that the porphin is desorbed intact from the surface. This is the first time that PDMS has been successfully utilized for direct detection of a high-molecular-weight adsorbate on a high-surface-area (catalyst) support. A peak corresponding to the metal-free porphin (615 Da) is observed in the positive ion spectrum of each adsorbed complex. This does not imply a surface-induced change since the PDMS spectra for the pure porphins gave the same fragmentation patterns. We suspect that incomplete conversion of the H_2-TPP to M-TPP is the source of this observation but cannot rule out contributions from demetallation or reassociation during the desorption/ionization process. We also note that these samples contain molecular aggregates on the surface and that their influence, as opposed to that of isolated adsorbed molecules, has not yet been de-

TABLE 1

Micropore Volume Measurements

Sample	Pretreatment temp.[a] (°C)	Micropore volume (cc/g)
Nd–Y zeolite	110	0.232
5 wt% Ni-TPP/Nd–Y	110	0.094
	110[b]	0.226

[a] Before measurement sample held at pretreatment temperature for 6 h at approximately 10^{-4} Torr.

[b] Sample calcined at 500°C in air for 4 h to decompose porphin before beginning pretreatment.

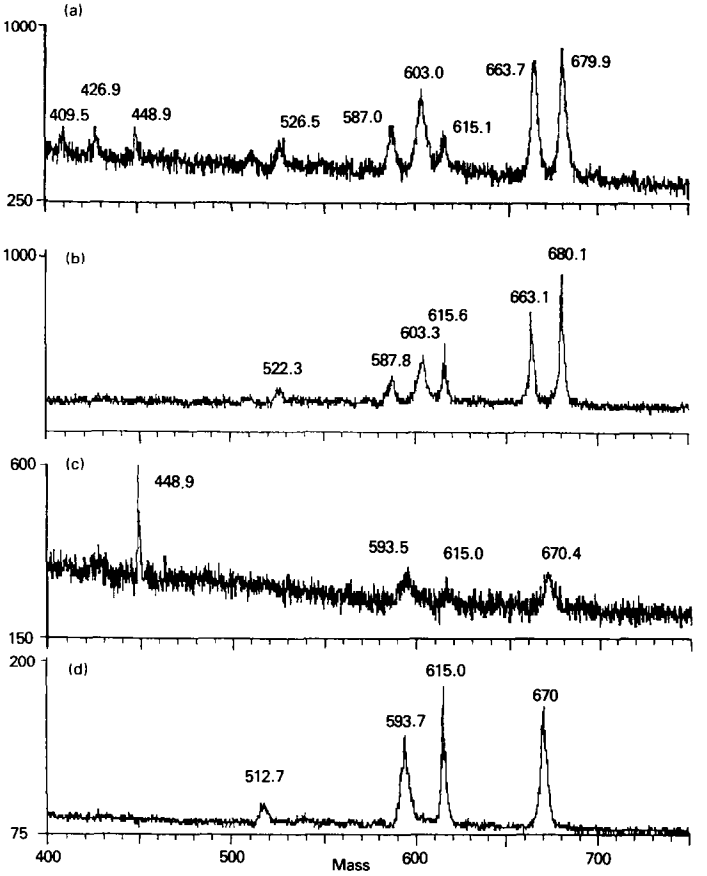

FIG. 8. Plasma desorption–mass spectra of (a) 8.0 wt% VO-TPP adsorbed on amorphous silica–alumina, (b) pure VO-TPP, (c) 5.0 wt% Ni-TPP adsorbed on amorphous silica–alumina, and (d) pure Ni-TPP.

termined. The PDMS spectra will be discussed in more detail elsewhere (*45*).

EPR analysis of adsorbed VO-TPP. The vanadium atom in VO-porphin is in a $^2B_2$ electronic term state (+4 oxidation state). Due to the single unpaired electron, it is easily observed by electron paramagnetic resonance (EPR) spectroscopy. At low loadings on amorphous silica–alumina or Nd zeolite, the room temperature EPR spectrum of adsorbed VO-TPP is similar to that observed at 77 K for VO-TPP in a frozen THF matrix (*46*). In Fig. 9*b*, for high-loading VO-TPP/amorphous silica–alumina at room temperature, the observed anisotropic spectrum of an immobile, molecularly isolated, tetragonally distorted V^{4+} complex is identical to that found at lower loadings. A similar spectrum has been observed for VO-etioporphin adsorbed on a HDS catalyst (*47*).

Figure 9*c*, for high-loading VO-TPP/Nd–Y zeolite, shows evidence for dipolar broadening of the individual hyperfine components due to a nearby paramagnetic center, either Nd^{3+} or another V^{4+} ion in close proximity. The EPR spectrum of solid-state, crystalline VO-TPP, Fig. 9*a*, was found to be indentical to that in Fig. 9*c* except for the sharp $g = 2.0$ line due to a paramagnetic impurity present in the zeolite. This is a carbonaceous residue formed

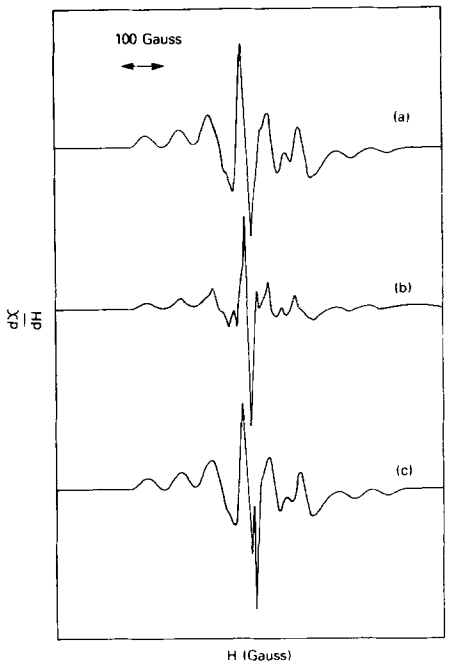

FIG. 9. Electron paramagnetic resonance spectra of (a) crystalline VO-TPP and 8.0 wt% VO-TPP adsorbed on (b) amorphous silica–alumina and (c) Nd–Y zeolite.

during the removal of toluene by drying at 393 K. Since the dipolar broadening effect is not observed at low (submonolayer) loadings, it must be attributed to VO^{2+}–VO^{2+} interactions rather than Nd^{2+} – VO^{2+} interactions. From the X-ray crystallographic parameters (*48*), the V–V nearest approach in VO-TPP is 8.677 Å, close enough to cause the line broadening observed. Thus, EPR analysis gives evidence for molecular aggregation of porphin deposited on the zeolitic support, but not on the amorphous support.

XPS analysis of adsorbed metalloporphins. The ground-state electronic properties of metalloporphins adsorbed on carbon black (*49*), montmorillonite (*50*), and HDS catalysts (*43*) have been examined previously by X-ray photoelectron spectroscopy (XPS). In Fig. 10, the N 1*s* and Ni $2p_{3/2}$ spectra for 5 wt% Ni-TPP adsorbed on amorphous silica–alumina and Nd–Y zeolite are compared. The characteristic spectra for molecular Ni-TPP (*51*) can be easily seen in the sample supported on amorphous silica–alumina, where the Ni $2p_{3/2}$ line at 853.2 eV and the N 1*s* line at 397.8 eV are the values expected for the pure porphin (see Table 2). The other nitrogen signal is caused by a surface nitrogen impurity also observed on the supports without porphins. The sample with the same loading of Ni-TPP deposited on Nd–Y exhibits a substantially lower level of detectable porphin, however, XPS does not give evidence for

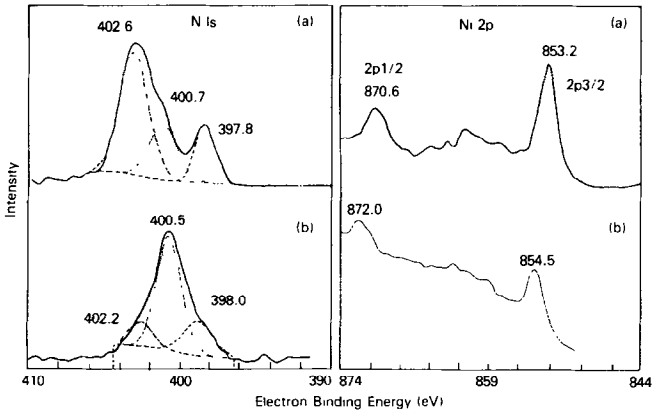

FIG. 10. X-ray photoelectron spectra of the N 1*s* and Ni $2p_{3/2}$ photoelectron lines for 5.0 wt% Ni-TPP adsorbed on (a) amorphous silica–alumina and (b) Nd–Y zeolite.

TABLE 2

Corrected XPS Binding Energies[a]

Sample	Al 2*p*	O 1*s*	C 1*s*	N 1*s*	M $2p_{3/2}$
Amorphous silica–alumina (Amor)	74.6	532.0	284.7	400.8, 402.4	
Nd–Y zeolite	74.7	531.8	284.5	400.4, 402.3	
15% Nd–Y FCC catalyst	74.5	531.6	284.8	401.8	
Ni-TPP[b]		531.6	284.6	397.8	854.3
Ni-TPP/Amor	74.5	531.6	283.8	397.8, 400.7, 402.6	853.2
Ni-TPP/Nd–Y	74.7	531.8	284.4	398.0, 400.5, 402.2	854.5
Ni-TPP/15% Nd–Y	74.8	532.0	283.6	397.7, 401.1, 402.6	854.1
VO-TPP[b]		531.2 534.0	284.6	397.8	515.1
VO-TPP/Amor	74.3	531.8	284.2	397.8, 401.0, 402.6	514.6
VO-TPP/Nd–Y	74.7	531.8	284.4	397.9, 400.2	515.3
VO-TPP/15% Nd–Y	74.2	530.7	282.4	397.8, 400.8, 402.7	515.3

[a] All binding energies corrected to Si 2*p* = 102.8 eV.
[b] Pure prophin binding energies corrected to C 1*s* = 284.6 eV.

demetallation and formation of a 399.1 eV N 1*s* signal characteristic of H_2-TPP or H_4-TPP^{2+} (*51–53*).

This general trend is also observed in Fig. 11 for adsorbed VO-TPP. The N 1*s* line at 397.8 eV is prominent for 8 wt% VO-TPP adsorbed on amorphous silica–alumina. The relative surface atomic percentages in Table 3, determined after accounting for differences in signal intensity, photoemission cross section, and electron escape depth, show that the surface vanadium concentration on amorphous silica–alumina is three times higher than that found on Nd–Y zeolite for the same loading of VO-TPP.

The two hypotheses presented previ-

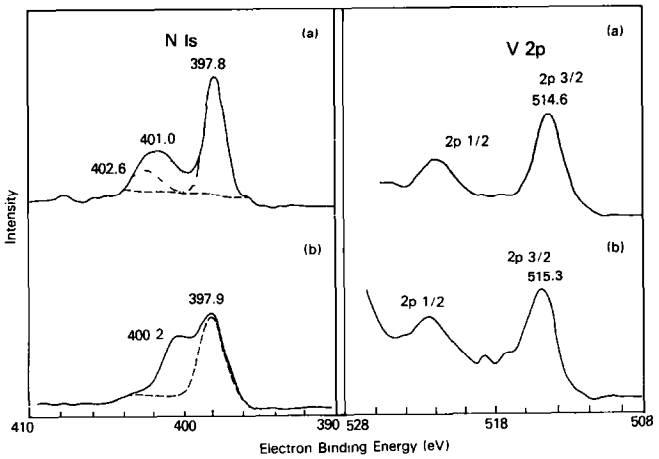

FIG. 11. X-ray photoelectron spectra of the N 1*s* and V $2p_{3/2}$ photoelectron lines for 8.0 wt% VO-TPP adsorbed on (a) amorphous silica–alumina and (b) Nd–Y zeolite.

TABLE 3

Relative Surface Atomic Percentages as Measured by XPS

Sample	C	O	Al	Si	N	Ni	V
Amorphous silica–alumina (Amor)	5.2	64.0	8.5	20.8	1.5		
Nd–Y zeolite	8.7	61.9	8.3	19.2	0.37		
15% Nd–Y FCC catalyst	4.5	64.7	9.0	20.2	1.2		
Ni-TPP/Amor	10.5	61.6	8.0	18.3	1.8	0.10	
Ni-TPP/Nd–Y	16.9	56.8	7.3	17.9	1.1	0.03	
Ni-TPP/15% Nd–Y	14.8	57.4	7.6	18.0	2.0	0.19	
VO-TPP/Amor	27.6	47.4	6.5	15.1	3.1		0.39
VO-TPP/Nd–Y	26.6	49.7	6.3	15.5	1.8		0.13
VO-TPP/15% Nd–Y	22.4	51.7	6.7	15.9	3.0		0.35

ously for porphin deposition and aggregation on the low external surface area zeolite were encapsulation via formation of multilayers and alternatively, porphin crystallite formation. At these high loadings the formation of five to eight monolayers (25–40 Å) would greatly diminish the observation of the silicon and aluminium in the support by the surface-sensitive XPS technique. However, the level of observable Si and Al is nearly the same as that found in the pure support. Therefore, it may be concluded that a large fraction of the added porphin must have condensed into porphin crystallites leaving less than one monolayer of porphin on the external surface of the zeolite. This hypothesis explains the low level of "observed" metal, since a large fraction would be effectively buried inside the porphin crystallite and thus would be inaccessible to this surface analytical technique.

SEM of aluminosilicates impregnated with metalloporphins. Further evidence for porphin crystallite formation during impregnation of zeolite-only supports has been obtained from electron microscopy analysis of Ni-TPP/zeolite samples (see Fig. 12). The standard crystalline morphology of the Y zeolite is micron-sized multi-

FIG. 12. Scanning electron micrograph of a Ni-containing particle found in 5.0 wt% Ni-TPP adsorbed on Nd–Y zeolite sample.

crystalline aggregates composed of individual crystallites 10–20 millimicrons in diameter (*54*). A few other large (~10 μm) irregularly shaped crystallites were also observed. Energy-dispersive X-ray (EDX) microanalysis of the zeolitic region showed typical Si, Al analyses but no Ni could be detected. Analysis of the 10-μm particles revealed high concentrations of Ni, implying a Ni-porphin crystallite. Similar analysis of amorphous silica–alumina-impregnated samples showed no uniform particle morphology and particle size varied from 5 to 60 μm. Again, no Ni could be detected in the EDX analysis, since the concentration of Ni is less than 1 at.%.

Metalloporphin impregnation of 15% Nd–Y FCC catalyst. As would be predicted on the basis of available surface area, impregnation of porphin on a support composed of 85% amorphous silica–alumina results in nearly uniform distribution across the catalyst surface. EPR analysis of adsorbed VO-TPP shows a spectrum identical to that in Fig. 9*b* for VO-TPP adsorbed on pure amorphous silica–alumina. XPS results as seen in Table 2 are also similar to those discussed previously for high porphin loading on the amorphous silica–alumina. The zeolite component does not appear to affect the initial deposition of porphin. The effect of its presence on the decomposition of the porphins, and the subsequent status of the Ni and V, will now be addressed.

Thermal analyses. The decomposition of supported metalloporphins was observed to be a function of the chelated metal as well as the type of support. In air, at 5°C/min, relatively sharp exotherms were observed for VO-TPP and Ni-TPP on Nd–Y zeolite, Fig. 13. However, metalloporphins supported on amorphous silica–alumina exhibit broad exotherms extending over a 150°C temperature range. Complementary information was obtained by TGA as shown in Fig. 14. The sample with 8 wt% VO-TPP adsorbed on Nd–Y zeolite exhibited an initial weight loss between 100 and 200°C due to water desorption, followed by a

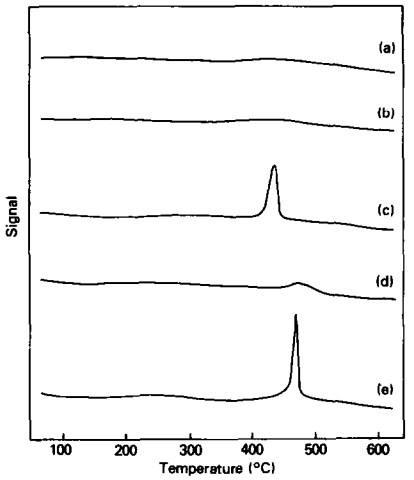

FIG. 13. Differential thermal analyses of 2- to 3-mg samples at a heating rate of 5°C/min in air. (a) 8 wt% VO-TPP adsorbed on 15% Nd–Y FCC catalyst; (b) 8 wt% VO-TPP adsorbed on amorphous silica–alumina; (c) 8 wt% VO-TPP adsorbed on Nd–Y zeolite; (d) 5 wt% Ni-TPP adsorbed on Nd–Y zeolite; and (e) 5 wt% Ni-TPP and 8 wt% VO-TPP adsorbed on Nd–Y zeolite.

dramatic 8% weight loss at ~400°C. This is exactly the same temperature as the exotherm found in the DTA experiment. For the same 8 wt% VO-TPP loading on amorphous silica–alumina, after the initial weight loss of adsorbed water, the porphin decomposition begins at ~400°C but extends over at least a 150°C temperature range as indicated by DTA.

Two possible explanations for the difference in thermal profile as a function of support may be proposed, based on known differences in the samples. Either the chemical properties of the support or the difference in porphin distributions may potentially affect the decomposition pathway. To test the hypothesis that prophin crystallites, observed by SEM on the pure zeolitic supports, are responsible for the sharp exotherms, physical mixtures of porphin and the two supports were prepared. DTA analyses of these samples, prepared to the same weight percent ratio, exhibited a sharp exotherm only in the case of the zeolite sup-

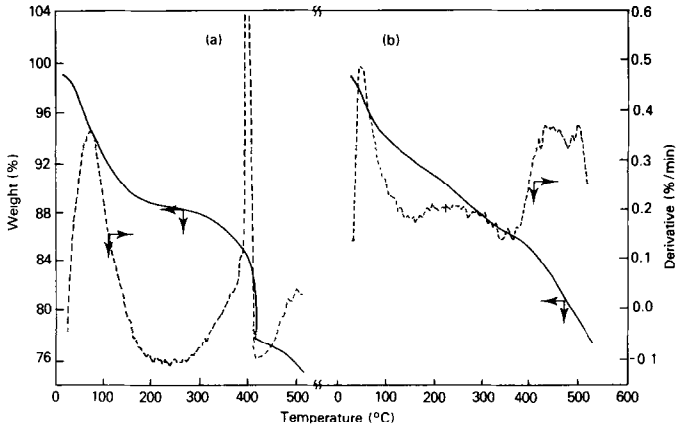

FIG. 14. Thermal gravimetric analyses of 10-mg samples at a heating rate of 5°C/min. (a) 8 wt% VO-TPP adsorbed on Nd–Y zeolite and (b) 8 wt% VO-TPP adsorbed on amorphous silica–alumina.

port. The conclusion may then be drawn that the zeolite support serves as a catalyst for the oxidative decomposition of the adsorbed species.

However, the 50°C difference in decomposition temperature as a function of metal suggests the possibility of a metal-catalyzed oxidation process. To substantiate this hypothesis, thermal analysis was performed on metal-free porphin supported on Nd–Y zeolite. Surprisingly, the 7 wt% H_2-TPP sample did not exhibit a sharp exotherm. The implications of this result are that both a catalytic metal and the zeolite support are required for catalytic, oxidative decomposition of the porphin ligand. Another interesting result was obtained when both Ni-TPP and VO-TPP were simultaneously impregnated on Nd–Y zeolite. DTA analysis of this sample revealed a very sharp exotherm similar to that for the VO-TPP decomposition, but displaced to the decomposition temperature of Ni-TPP. One explanation of this result is that the metals interact after porphin decomposition but before the onset of the oxidation reaction.

The peak maximum in the DTA for decomposition of metalloporphins on Nd–Y was found to vary as a function of heating rate. It is well known that the rate of temperature rise has a significant effect on peak temperature for reactions involving loss in weight or chemical reaction with the surrounding gas (*55*). If the data are analyzed using first-order kinetic theory (*56*), Eq. (1) can be derived for the relationship between the observed peak maximum (T_{max}) and the heating rate (ϕ):

$$\ln[\phi/T_{max}^2] = -E_a/R \cdot 1/T_{max} + \ln(AR/E_a]. \quad (1)$$

A in Eq. (1) is a constant. The values for the activation energies of decomposition, E_a, obtained from the slopes in Fig. 15 show that Ni-TPP (E_a = 32.5 kcal/mole) is more

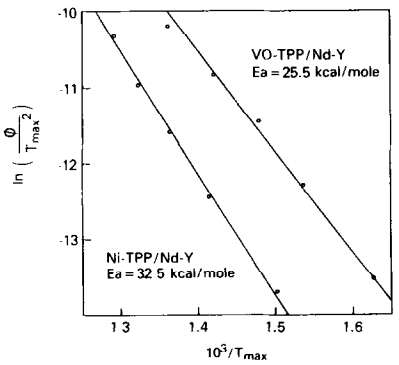

FIG. 15. Heating rate/T_{max}^2 versus $1/T_{max}$ for the differential thermal analyses of Ni-TPP and VO-TPP at heating rates between 0.5 and 20°C/min.

stable than VO-TPP (E_a = 25.5 kcal/mole). This difference in apparent thermal stability, clearly seen in Fig. 13, has been noted previously (*18*). At 8°C/min heating rate, Pompe *et al.* (*18*) observed the decomposition of an undisclosed Ni-porphin at an approximately 100°C higher temperature than for the V-porphin. Perhaps this result is a consequence of vanadium being a better oxidation catalyst than nickel under these conditions.

On the mixed support, the decomposition profile was similar to that observed on pure amorphous silica–alumina. This important finding implies that when the porphin is well distributed, the DTA calcination treatment does not result in a substantial metal–zeolite interaction, and therefore, sharp exotherms are not observed.

In an attempt to obtain spectroscopic evidence for decomposition of the supported metalloporphins as a function of temperature, FT-IR spectra were obtained for calcined samples. As shown in Fig. 16, aluminosilicates exhibit a broad absorption centered around 1050 cm^{-1} due to tetrahedral AlO_4 and/or SiO_4 asymmetric stretching modes (*57*). Only amorphous silica–alumina was used in this study because zeolitic materials have bands in the 700 to 800-cm^{-1} region due to framework double-six-ring deformations (*57*) which interfere with identification of adsorbed porphin. In Fig. 16*a*, the sharp bands above the background are due to porphin ring deformations (*58, 59*). The band at 1000 cm^{-1} is due to V–O stretching (*60*). After 300°C calcination, the bands associated with intact porphin have disappeared, indicating loss of the conjugated ring structure. It is important to note that this is substantially below the lowest exotherm observed in the DTA, implying that porphin ring decomposition occurs well before catalytic oxidation of the resulting carbonaceous material. The absence of adsorbate-dependent bands in the 1580 to 1620-cm^{-1} region (not shown) of spectra 16*c* and 16*d* indicates that heating in air does not produce the coke species found

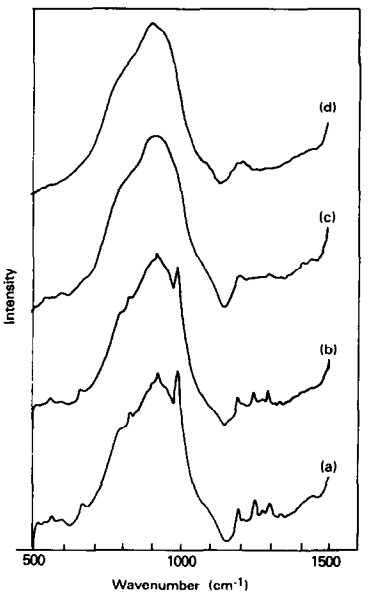

FIG. 16. Fourier transform infrared spectra of VO-TPP adsorbed on amorphous silica–alumina and calcined at (a) 100°C, (b) 200°C, (c) 300°C, and (d) 400°C in air for 1 h.

when VO-TPP is heated to 300°C and above in H_2 (*61*). Streusand and Schrader (*40*) obtained resonance Raman spectra of Ni-TPP adsrobed on γ-alumina and silica. Heating at 300°C in N_2 resulted in the loss of signal intensity indicating decomposition of porphin. Appearance of new bands provided evidence for an intermediate on γ-alumina after only 15 min heating. This unidentified signal may be related to the porphin decomposition product identified by Agrawal and Wei (*31*) and Ware and Wei (*32*) for the decomposition of Ni-TPP on HDS catalysts.

XPS analysis of metal poisons following porphin decomposition. The chemical state of the metal contaminants on FCC catalysts has been examined by X-ray photoelectron spectroscopy in a recent study (*34*). A sample with 2.3% Ni showed only oxidized Ni. A sample with 1.9% V showed the presence of both V^{4+} and V^{5+} under cracking conditions, but in a decoked catalyst the vanadium was observed only in the V^{5+} state (*34*).

TABLE 4

Corrected XPS Binding Energies[a] after 500°C Calcination

	Al 2*p*	O 1*s*	C 1*s*	N 1*s*	M $2p_{3/2}$
Ni-TPP/Amor	74.7	531.8	284.6	400.3, 401.9	857.0
Ni-TPP/Nd–Y	74.4	531.7	284.4	399.4, 401.1	857.8
Ni-TPP/15% Nd–Y	74.7	531.7	284.8	400.6, 402.3	856.8
VO-TPP/Amor	74.7	532.2	285.0	400.5	516.3, 517.9
VO-TPP/Nd–Y	74.8	531.8	285.0	400.8, 402.7	516.4, 517.6
VO-TPP/15% Nd–Y	74.7	531.9	285.0	398.5, 399.5, 401.1	515.5, 517.0

[a] All binding energies corrected to Si 2*p* = 102.8 eV.

In the present study, aluminosilicate supports were impregnated with 5 wt% Ni-TPP and 8 wt% VO-TPP. Calcination at 500°C resulted in porphin decomposition, coke combustion, and metal deposition on the catalyst surface. The resulting aluminosilicates contained approximately 5000 ppm Ni and 8000 ppm V. XPS analysis of the Ni $2p_{3/2}$ line showed binding energies between 856.8 and 857.8 eV on all supports. When silica–alumina was present, Ni $2p_{3/2}$ binding energies of 856.9 ± 0.1 eV were found, indicative of Ni^{2+}, possibly as $NiAl_2O_4$ (*62, 63*) (see Table 4). On Nd–Y, the Ni $2p_{3/2}$ line was at an unusually high energy of 857.8 eV, but contributions of oxidation state, matrix effects, and relaxation have not been evaluated. The oxidation state of vanadium, however, was found to be a mixture of V^{4+} and V^{5+} as shown in Fig. 17. On amorphous silica–alumina, the ratio was approximately 1 : 1, but on Nd–Y zeolite approximately 85% of the vanadium was in the V^{5+} form. When impregnated on the mixed support, the porphin was well dispersed and the vanadium was again not completely oxidized to V^{5+}.

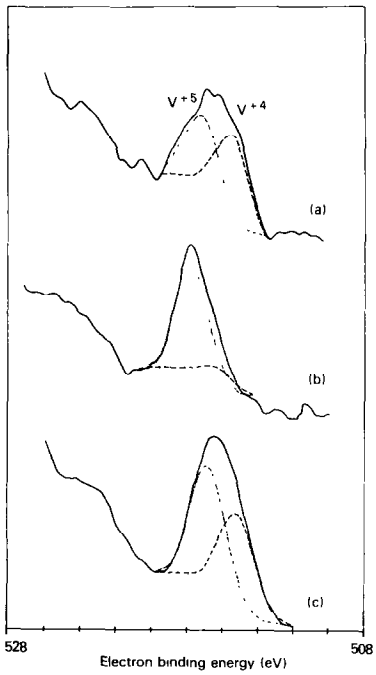

FIG. 17. X-ray photoelectron spectra of the V $2p_{3/2}$ line for 8 wt% VO-TPP adsorbed on (a) amorphous silica–alumina, (b) Nd–Y zeolite, and (c) 15% Nd–Y FCC catalyst all following calcination at 500°C for 4 h.

In Table 5 are listed the surface atomic percentages found by XPS following porphin decomposition. The quantity of observable metal does not change appreciably compared to values for the original samples (Table 3) on either amorphous silica–

TABLE 5

Relative Surface Atomic Percentages as Measured by XPS after 500°C Calcination

	C	O	Al	Si	N	Ni	V
Ni-TPP/Amor	6.0	62.3	9.1	22.0	0.5	0.12	
Ni-TPP/Nd–Y	8.9	62.5	7.7	20.0	0.4	0.5	
Ni-TPP/15% Nd–Y	5.3	64.1	8.2	21.7	0.7	0.08	
VO-TPP/Amor	5.8	62.3	8.7	22.5	0.4		0.25
VO-TPP/Nd–Y	7.0	64.4	7.4	21.2	0.25		0.36
VO-TPP/15% Nd–Y	11.0	60.5	8.3	20.6	0.6		0.24

alumina or the mixed support. On the zeolitic support, however, the metal on the surface appears to increase substantially after decomposition. This observation can again be explained as resulting from the release of metal ions from the decomposing porphin crystallites onto the surface of the zeolite.

CONCLUSIONS

Deposition of Ni-TPP and VO-TPP on the individual components of FCC catalysts has been investigated as a function of loading. At low loading (~0.2 wt % porphin) EPAS and EPR determine that the porphin is molecularly distributed on the surface. Changes in the relative intensity of the Soret and visible bands imply that the surface is slightly distorting the molecular structure.

At high loadings (5 wt% Ni-TPP or 8 wt% VO-TPP) on armorphous silica–alumina there is enough available surface area to retain molecular distribution. The EPA spectra are consistent with multilayer formation, but EPR spectroscopy of supported VO-TPP shows the vanadium to be tetragonally distorted but still molecularly isolated from nearby paramagnetic centers. Therefore, the EPA spectra must arise from a distortion of the molecular symmetry induced by the surface. XPS results are consistent with the presence of metal porphins and not metal-free porphin. PDMS, which indicates that the porphins are intact on the surface, may also prove to be a useful analytical tool for investigation of adsorbates on other solid and/or catalytic surfaces.

At high loadings on Y zeolite, there is not enough surface area to molecularly disperse all the porphin. The EPAS and EPR spectra are consistent with the formation of multilayers or crystalline aggregates. The intensity of the Soret band, however, implies that a fraction of the porphin is not involved in crystallites. The observation of large quantities of silicon and aluminium in XPS analysis eliminates the presence of porphin multilayers as a possible deposition profile. The pore blockage observed in micropore analysis shows, however, that there could be nearly one monolayer on 60% of the crystalline aggregates. Furthermore, actual porphine crystallites have been observed by SEM. All these results are consistent with the following deposition scenario: in the initial stages of deposition the porphin deposits on the surface of the zeolitic aggregates; however, after most of the available space is consumed the porphins preferentially self-condense into crystallites rather than form multilayers.

Infrared analyses of adsorbed metalloporphins calcined in air indicate that the porphin loses its aromatic ring structure between 200 and 300°C. Thermal analyses (DTA and TGA) show that metalloporphins deposited on a zeolitic support decompose in air over a narrow temperature range. This rapid decomposition is not observed on amorphous supports or for metal-free porphin, implying that a chelated metal and a zeolitic support are both required for catalytic oxidation of the organic residue produced by porphin decomposition. The differences between nickel and vanadyl-TPP can be attributed to the better catalytic oxidative properties of vanadium.

Analysis of the chemical state of the metals following porphin decomposition shows that the nickel is in the form of Ni^{2+} in the presence of silica–alumina and is oxidized to at least the 2+ state on the zeolites, while the oxidation state of vanadium is clearly dependent on the support with the zeolitic support producing more V^{5+}.

ACKNOWLEDGMENTS

We thank Amoco Oil Co. and the U.S. Department of Energy, BES-Materials Sciences (Contract W-31-109-ENG-38), for their support of this work; J. E. Hunt, Argonne, for collaboration on the PDMS experiments; and C. L. Caenepeel, Amoco, for useful discussions.

REFERENCES

1. Tolen, D. F. *Oil Gas J.* **79**(13), 90 (1981).
2. Ritter, R. E., Rheaume, L. Welsh, W. A., and Magee, J. S., *Oil Gas J.* **79**(27), 103 (1981).

3. Upson, L. L., *Hydrocarbon Process.* **60**(11), 253 (1981).
4. Duffy, B. J., and Hart, H. M., Chem. Eng. Prog. **48**(7), 344 (1952).
5. Donaldson, R. E., Rice, T., and Murphy, J. R., *Amer. Chem. Soc. Div. Pet. Chem. B*, 97 (1960).
6. Meisenheimer, R. G., *J. Catal.* **1,** 356 (1962).
7. Cimbalo, R. N., Foster, R. L., and Wachtel, S. J., *Oil Gas J.* **70**(20), 112 (1972).
8. Mills, G. R., *Ind. Eng. Chem.* **42,** 182 (1950).
9. McIntosh, C. H. *Amer. Chem. Soc. Div. Pet. Chem.* **32,** 113 (1954).
10. Rothrock, J. J., Birkhimer, E. R., and Leum, L. N., *Ind. Eng. Chem.* **49,** 272 (1957).
11. Connor, J. E, Rothrock, J. J., Birkhimer, E. R., and Leum, L. N., *Ind. Eng. Chem.* **49,** 276 (1957).
12. Habib, E. T., Owen, H. Synder, P. W., Streed, C. W., and Venuto, P. B., *Ind. Eng. Chem. Prod. Res. Dev.* **16,** 291 (1977).
13. Mitchel, B. R., *Ind. Eng. Chem. Prod. Res. Dev.* **19,** 209 (1980).
14. Chester, A. W., *Amer. Chem. Soc. Div. Pet. Chem.* **26,** 505 (1981).
15. Järås, S., *Appl. Catal.* **2,** 207 (1982).
16. Nishimura, Y., Masuda, T. Sato, G., and Egashira, S., *Amer. Chem. Soc. Div. Pet. Chem.* **28,** 707 (1983).
17. Speronello, B. K., and Reagan, W. J., *Oil Gas J.* **82**(5), 139 (1984).
18. Pompe, R., Järås, S., and Vannerberg, N-G., *Appl. Catal.* **3,** 171 (1984).
19. Wormsbecher, R. F., Peters, A. W., and Maselli, J. M., *J. Catal.* **100,** 130 (1986).
20. Marriott, P. J., Gill, J. P., Evershed, R. P., Hill, C. S., and Eglinton, G., *J. Chromatogr.* **301,** 107 (1984).
21. Wolff, G. A., Chicarelli, M. I., Shaw, G. J., Evershed, R. P., Quirke, J. M. E., and Maxwell, J. R., *Tetrahedron* **40,** 3786 (1984).
22. Magee, J. S., and Blazek, J. J., *ACS Monogr.* **171,** 615 (1976).
23. Adler, A. D., Longo, F. R., and Kampas, F., *J. Inorg. Nucl. Chem.* **32,** 2443 (1970).
24. Adler, A. D., Longo, F. R., and Varadi, V., *Inorg. Synth.* **16,** 213 (1976).
25. Klug, H. P., and Alexander, L. E., "X-ray Diffraction Procedures for Polycrystalline and Amorphous Materials," pp. 410–415. Wiley, New York, (1974).
26. Brunauer, S. Emmett, P. H., and Teller, E. J., *J. Amer. Chem. Soc.* **60,** 309 (1938).
27. Roberts, B. F. J., *J. Colloid Interface Sci.* **23,** 266 (1967).
28. Gregg, S. J., and Sing, K. S. W., "Adsorption, Surface Area, and Porosity," pp. 214–216. Academic Press, New York, 1982.
29. Hunt, J. E., Schaber, P. M., Michalski, T. J., Dougherty, R. C., and Katz, J. J., *Int. J. Mass. Spectrom. Ion Phys.* **53,** 45 (1983).
30. Hung. C. W., and Wei, J., *Ind. Eng. Chem. Process Des. Dev.* **19,** 250, 257 (1980).
31. Agrawal, R., and Wei, J., *Ind. Eng. Chem. Process Des. Dev.* **23,** 505, 515 (1984).
32. Ware, R. A., and Wei, J., *J. Catal.* **93,** 100, 122, 135 (1985).
33. Parks, G. D., Schaffer, A. M., Dreiling, M. J., and Shiblom, C. M., *Amer. Chem. Soc. Div. Pet. Chem.* **25,** 334 (1980).
34. Anderson, S. L. T., Lundin, S. T., Järås, S., and Otterstedt, J. E., *Appl. Catal.* **9,** 317 (1984).
35. Carnall, W. T., Fields, P. R., and Wybourno, B. G., *J. Chem. Phys.* **42,** 3797 (1965).
36. Carnall, W. T., Fields, P. R., and Rajnak, K., *J. Chem. Phys.* **49,** 4424 (1968).
37. Gouterman, M., *J. Mol. Spectrosc.* **6,** 138 (1961).
38. Weiss, C., Kobayashi, H., and Gouterman, M., *J. Mol. Spectrosc.* **16,** 415 (1965).
39. Edwards, L., Dolphin, D. H., Gouterman, M., and Adler, A. D., *J. Mol. Spectrosc.* **38,** 16 (1971).
40. Streusand, B. J., and Schrader, G. L., *Appl. Spectrosc.* **38,** 433 (1984).
41. Tsuji, K., Imaizumi, M., Oyoshi, A., Mochida, J., Fujitsu, H., and Takeshita, K., *Inorg. Chem.* **21,** 721 (1982).
42. Mochida, I., Tsufi, K., Suctsugu, K., Fujitsu, H., and Takeshita, K., *J. Phys. Chem.* **84,** 3159 (1980).
43. Mitchell, P. C. H., Scott, C. E., Bonnelle, J. P., and Grimbolt, J. G., *J. Chem. Soc. Faraday Trans. 1* **81,** 1047 (1985).
44. Rosencwaig, G., and Gersho, A., *J. Appl. Phys.* **47,** 64 (1976).
45. Hunt, J. E., and Roth, S. A., to be published.
46. Kivelson, D., and Lee, S. K., *J. Chem. Phys.* **41,** 1896 (1964).
47. Mitchell, P. C. H., and Scott, C. E., *Actas Simp. Iberoam. Catal. 9th* **2,** 1303 (1984).
48. Drew, M. G. B., Mitchell, P. C. H., and Scott, C. E., *Inorg. Chim. Acta* **82,** 63 (1984).
49. Van Veen, J. A. R., Van Boar, J. F., and Kroese, K. J., *J. Chem. Soc. Faraday Trans. 1* **77,** 2827 (1981).
50. Canesson, P., Cruz, M. I., and Van Damme, H., *Dev. Sedimentol.* **27,** 217 (1979).
51. Karweik, D. H., and Winograd, N., *Inorg. Chem.* **15,** 2336 (1976).
52. Zeller, M. V., and Hayes, R. G., *J. Amer. Chem. Soc.* **95,** 3855 (1973).
53. Nina, Y., Kobayashi, H., and Tsuchiya, T., *J. Chem. Phys.* **60,** 796 (1974).
54. Breck, D. W., "Zeolite Molecular Sieves," p. 277. Wiley, New York, 1974.
55. Garn, P. D., "Thermoanalytical Methods of Investigation," pp. 57–61. Academic Press, New York 1985.
56. Boudart, M., and Djega-Mariadassou, G., "Kinetics of Heterogeneous Catalytic Reactions," p. 60. Princeton Univ. Press, Princeton, 1984.

57. Flanigen, E. M., *ACS Monogr.* **171,** 81 (1986).
58. Thomas, D. W., and Martell, A. E., *J. Amer. Chem. Soc.* **81,** 5111 (1959).
59. Ogoshi, H., Saito, Y., and Nakamoto, K., *J. Chem. Phys.* **57,** 4194 (1972).
60. Burger, H., *in* "Phorphyrins and Metalloporphyrins." (K. M. Smith, Ed.), pp. 524–535. Elsevier, New York, 1975.
61. Vielhaber, B., and Knözinger, H., *Appl. Catal.* **26,** 375 (1986).
62. Wagner, C. D., "Handbook of X-Ray Photoelectron Spectroscopy," p. 80. Perkin–Elmer, 1979.
63. Fleisch, T. H., Winograd, N., and Delgass, W. N., *Surf. Sci.* **78,** 141 (1978).